ORCA – Online Research @ Cardiff

This is an Open Access document downloaded from ORCA, Cardiff University's institutional repository:https://orca.cardiff.ac.uk/id/eprint/135987/

This is the author's version of a work that was submitted to / accepted for publication.

Citation for final published version:

Hasentab, E., Tusch, J., Schnabel, C., Marien, C. S., Van Kranendonk, M. J., Smithies, H., Howard, H., Maier, W. D. and Munker, C. 2021. Evolution of the early to late Archean mantle from Hf-Nd-Ce isotope systematics in basalts and komatiites from the Pilbara Craton. Earth and Planetary Science Letters 553 , 116627. 10.1016/j.epsl.2020.116627

Publishers page: http://dx.doi.org/10.1016/j.epsl.2020.116627

Please note:
Changes made as a result of publishing processes such as copy-editing, formatting and page numbers may not be reflected in this version. For the definitive version of this publication, please refer to the published source. You are advised to consult the publisher's version if you wish to cite this paper.

This version is being made available in accordance with publisher policies. See http://orca.cf.ac.uk/policies.html for usage policies. Copyright and moral rights for publications made available in ORCA are retained by the copyright holders.

Evolution of the early to late Archean mantle from Hf-Nd-Ce isotope systematics in basalts and komatiites from the Pilbara Craton

E. Hasenstab[1*], J. Tusch[1], C.Schnabel[1,2], C. S. Marien[1], M. J. Van Kranendonk[3], H. Smithies[4], H. Howard[4], W. D. Maier[5], C. Münker[1]

[1]Institut für Geologie und Mineralogie, Universität zu Köln, Zülpicher Straße 49, 50674 Cologne, Germany

[2]Abteilung Nuklearchemie, Universität zu Köln, Zülpicher Straße 45, 50674 Cologne, Germany

[3]Australian Centre for Astrobiology, University of New South Wales, Kensington, NSW 2052, Australia

[4]Geological Survey of Western Australia, Mineral House, 100 Plain Street, East Perth, WA 6004, Australia

[5]School of Earth and Ocean Sciences, Cardiff University, Main Building, Park Place, Cardiff CF10 3AT, United Kingdom

[*]Corresponding author at: Universität zu Köln, Institut für Geologie und Mineralogie, Zülpicher Str. 49b, 50674 Köln, Germany.

Tel,: +49 221 470-89866

E-Mail address: ehasens1@uni-koeln.de

Keywords: Archean; Hadean; Pilbara; komatiites; Hf-Nd; Ce-Nd; Lu-Hf; Sm-Nd; La-Ce; decoupling; differentiation

Abstract

Inferences on the early evolution of the Earth's mantle can be deduced of long-lived radiogenic isotope systems such as ^{176}Lu-^{176}Hf and ^{147}Sm-^{143}Nd, for which both parent and daughter elements largely remain immobile at low metamorphic grades. However, it remains ambiguous when and to what extent mantle-crust differentiation processes had started in the Archean. For a better understanding of Archean mantle-crust evolution, we determined the initial ^{176}Lu-^{176}Hf, ^{147}Sm-^{143}Nd, and, in a new approach, the ^{138}La-^{138}Ce isotope compositions of a suite of Archean mafic-ultramafic rock samples from the 3.53-2.83 Ga old Pilbara Craton and 2.78-2.63 Ga old Fortescue Group in NW Australia. These rocks represent one of the best-preserved Archean successions worldwide and contain mafic-ultramafic rocks that were erupted during repeated and long-lived pulses of volcanism throughout much of the Archean. Mantle-derived mafic-ultramafic rock samples were collected from six major stratigraphic groups of the Pilbara Craton and the overlying Fortescue Group in order to characterize the parental mantle source regions of the lavas and to reconstruct the temporal

evolution of the ambient mantle beneath this piece of cratonic lithosphere. In addition, we analyzed contemporaneous TTG-like igneous suites and interbedded sediments in order to reconstruct the lithospheric evolution of the Pilbara Craton.

The Hf-Nd-Ce isotope data imply the onset of mantle-crust differentiation in the Pilbara Craton as early as ~4.2 Ga, well prior to any of the preserved stratigraphy. Within error, coupled Ce-Nd-Hf isotope arrays all intersect chondritic values, implying that the Earth is of broadly chondritic composition, also for the ^{138}La-^{138}Ce isotope system. Mafic rocks usually yield strongly coupled $\varepsilon\mathrm{Hf}_{(i)}$, $\varepsilon\mathrm{Nd}_{(i)}$ and $\varepsilon\mathrm{Ce}_{(i)}$ values that form a mixing line between an evolving depleted upper mantle composition and the primitive mantle value ($\varepsilon\mathrm{Hf}_{(i)}$ ca. 0.0 to + 3.2, $\varepsilon\mathrm{Nd}_{(i)}$ ca. +0.2 to +1.7 and $\varepsilon\mathrm{Ce}_{(i)}$ ca. +0.3 to -0.1). As all Paleoarchean samples lack co-variations between Nb/Th with $\varepsilon\mathrm{Hf}_{(i)}$ or $\varepsilon\mathrm{Nd}_{(i)}$, contamination with an enriched crust is unlikely to explain this mixing trend. The most primitive mafic samples show elevated $\mathrm{Gd_N/Yb_N}$ ratios (2.2-1.4), implying the involvement of a deep-rooted, near-primitive, upwelling mantle that was progressively mixed into the depleted upper mantle. In contrast to the mafic rocks, most, but not all komatiites are decoupled in their initial Hf-Nd-Ce isotope compositions, by having extremely radiogenic $\varepsilon\mathrm{Hf}_{(i)}$ values at only moderately high $\varepsilon\mathrm{Nd}_{(i)}$ and low $\varepsilon\mathrm{Ce}_{(i)}$ values. This decoupling is best explained by the assimilation of mantle domains that underwent early melt depletion in the garnet stability field and evolved at high ^{176}Lu/^{176}Hf ratios but at moderate ^{147}Sm/^{143}Nd and ^{138}La/^{138}Ce ratios over time. The disappearance of rocks with decoupled Hf-Nd isotope compositions after ~3.2 Ga is likely linked to decreasing mantle temperatures that were no longer able to melt such refractory mantle domains. Collectively, our new data for mafic rocks from the Pilbara Craton confirms the presence of long-term depleted mantle domains in the early Archean that are not sampled by the zircon Hf isotope record in the Pilbara Craton.

1. Introduction

The ^{176}Lu-^{176}Hf and ^{147}Sm-^{143}Nd decay systems have become key analytical tools for reconstructing the early depletion history of the terrestrial mantle due to their robustness (e.g., Bennett et al., 1993; Vervoort and Blichert-Toft, 1999; Hoffmann et al., 2011b). In contrast, the ^{138}La-^{138}Ce system has only rarely been applied to the early terrestrial rock record, because the slow radiogenic decay of ^{138}La to ^{138}Ce (λ=2.37×10^{-12} a^{-1}) and limited fractionation of La/Ce in igneous systems result in small Ce isotope variations that are analytically difficult to resolve. During mantle-crust differentiation, Lu and Sm are more compatible in the mantle compared to Nd and Hf, whereas La is more incompatible in the mantle compared to Ce. Thus, depleted mantle domains will evolve towards positive initial $\varepsilon Hf_{(i)}$ and $\varepsilon Nd_{(i)}$, but towards negative $\varepsilon Ce_{(i)}$ values. Hence, ^{138}La-^{138}Ce systematics could, in principle, be applied to similar geochemical issues as the ^{176}Lu-^{177}Hf or ^{147}Sm-^{144}Nd systems. As a consequence, combined Ce-Nd-Hf isotope studies can place further constraints on early Earth differentiation processes such as the observed decoupling of Hf-Nd isotopes in Archean rocks (e.g. Hoffmann et al., 2011b; Rizo et al., 2011).

The Pilbara Craton is an excellent example to study the evolution of mantle-crust differentiation processes on early Earth, due to long-lived volcanic pulses of mafic-ultramafic volcanism (Van Kranendonk et al., 2002). For other cratons, such as the North Atlantic Craton, mantle evolution processes have been complicated by secondary metamorphic events, which can disturb the Hf-Nd isotope signatures of such highly metamorphosed rocks (e.g. Gruau et al., 1996; Hoffmann et al., 2011b). In contrast, the majority of rocks from the Pilbara Craton have only been affected by low-grade metamorphism, largely at lower greenschist facies and only locally at amphibolite facies conditions (Collins and Van Kranendonk, 1999; Van Kranendonk et al., 2002). Although there exist other cratons that contain older rocks, the well-preserved and low metamorphic grade lithostratigraphic successions in the Pilbara Craton provide a near-continuous record of igneous evolution for almost a billion years of Earth history, from 3.59-2.63 Ga (e.g., Van Kranendonk et al., 2002; Smithies et al., 2007a; Petersson et al., 2019).

Based on predominantly positive $\varepsilon Nd_{(i)}$ values, many studies on Pilbara mafic-ultramafic rock samples suggest a moderately depleted mantle reservoir as a source for the dominantly mafic-ultramafic greenstone belt stratigraphy (e.g., Gruau et al., 1987; Arndt et al., 2001; Smithies et al., 2007b). However, previously reported Hf isotope data challenged these interpretations (Nebel et al., 2014; Kemp et al., 2015; Petersson et al., 2019; Petersson et al., 2020). For example, studies on zircons by Kemp et al. (2015) and Petersson et al., (2019, 2020) argued that the mantle beneath the Pilbara Craton did not start to differentiate until ~3.6 Ga. In contrast Nebel et al. (2014) reported extremely radiogenic $\varepsilon Hf_{(i)}$ values in ~3.5-3.2 Ga komatiites, which requires a highly depleted mantle reservoir to have been present already in the Hadean, a conclusion previously also reached by Tessalina et al. (2010).

In this study, we present high-precision isotope dilution (ID) and isotope composition data for ^{176}Lu-^{176}Hf, ^{147}Sm-^{143}Nd and ^{138}La-^{138}Ce on a variety of rock samples from the Pilbara Craton in order to better understand the long-term depletion history of the ambient mantle beneath the evolving Pilbara Craton and the early Archean mantle in general. We analyzed 39 basalts and komatiites, five granitoids, and three sedimentary rocks that were previously studied by Tusch et al. (2020) for their major and trace element data, as well as for their ^{182}W isotope systematics. Furthermore, we analyzed six basalts from the Jeerinah Formation that were provided by the Geological Survey of Western Australia, as well as ten komatiites that were previously studied by Maier et al. (2009) for platinum group element (PGE) concentrations. In total, we present combined ^{176}Lu-^{176}Hf and ^{147}Sm-^{143}Nd systematics on 63 mantle-derived rocks, granitoids, and sediments. For a better understanding of the ^{138}La-^{138}Ce system in the Archean, we also report ^{138}La-^{138}Ce data for a subset of 40 of these samples. The data are evaluated with an emphasis on the temporal evolution of the Archean mantle and source domain characteristics.

2. Geological setting

The Pilbara Craton is located in the northwestern part of Western Australia and is composed of several distinct litho-tectonic terranes that contain thick successions of mafic-ultramafic and felsic volcanic rocks (Van Kranendonk et al., 2007). The volcanic rocks erupted in several episodes lasting from at least 3.59-2.63 Ga, accompanied by pulses of granitic magmatism over the range of 3.49-2.83 Ga. Typical dome-and-keel structures are preserved in the Paleoarchean nucleus of the East Pilbara Terrane (EPT) (Fig. 1) (Van Kranendonk et al., 2004). The oldest unambiguous evidence for magmatic activity in the Pilbara Craton is provided by 3.7-3.8 Ga inherited zircons (Van Kranendonk et al., 2002; Kemp et al., 2015) and recently Petersson et al. (2019) have identified gabbroic enclaves (3.59-3.58 Ga Mount Webber Gabbro) that may be remnants of a mafic proto-crust.

Between ca. 3.53 and 3.23 Ga, cycles of mafic-ultramafic volcanism dominated the evolution of the EPT, deposited in three unconformity-bound groups: the ca. 3.53-3.43 Ga Warrawoona Group, the ca. 3.35-3.32 Ga Kelly Group and the 3.27-3.235 Ga Sulphur Springs Group (Van Kranendonk et al., 2007; Hickman, 2012). From the increasingly thickened mafic crust, partial melts escaped and formed repeated generations of felsic intrusions (Smithies et al., 2007a; Van Kranendonk, 2010; Wiemer et al., 2018). The thickened mafic crust also acted as a thermal incubator, thus softening the middle crust and causing gravitational instabilities (e.g., Collins and Van Kranendonk, 1999; Wiemer et al., 2018). During gravitational collapse, the negatively buoyant overlaying mafic crust sank into the middle crust, which, in turn, caused the rise of felsic domes and the typical dome-and-keel geometry (Collins and Van Kranendonk, 1999; Van Kranendonk et al., 2004; Wiemer et al., 2018).

At ~3.2 Ga, plume-initiated rifting separated the Kurrana and Karratha terranes from the EPT, which led to the eruption of the 3.18 Ga Soanesville Group and the contemporaneous Dalton Suite of intrusive layered mafic-ultramafic rocks in the EPT (Van Kranendonk et al., 2007a, 2010). This rifting event was recently interpreted in favor of the onset of Phanerozoic-style plate tectonics, and the tectono-magmatic history of the craton between 2.9 and 3.2 Ga was interpreted to represent a full Wilson cycle between 3.2-2.9 Ga (Van Kranendonk et al., 2010). This also includes the ~3.12 Ga Whundo Group volcanics that provide evidence for subduction-related volcanism in the Pilbara Craton (Smithies et al., 2007c). Between 3.07 to 2.91 Ga, the West Pilbara Superterrane (WPS), the

EPT, and the southeastern Kurrana Terrane accreted during three orogenic events (Van Kranendonk et al., 2007), followed by deposition of the 3.02-2.92 Ga De Grey Supergroup in an extensional basin (Van Kranendonk et al., 2007; Hickman, 2012) that was coeval with 2.935 Ga granitoid intrusions of the Yule Granitic Complex. Volcanic rocks from the De Grey Supergroup show strongly enriched geochemical characteristics indicating enriched, metasomatized mantle sources of possible lithospheric mantle origin (Smithies et al., 2004).

Deposition of the 2.78-2.63 Ga Fortescue Group followed cratonization of the Pilbara Craton, which was completed by the emplacement of ca. 2.83 granitoid rocks (Van Kranendonk et al., 2007). The dominantly continental flood basaltic lavas of the Fortescue Group were fed by a series of large feeder dykes, including the 2.78 Ga Black Range dolerite suite that erupted lavas of the lowermost Mount Roe basalt (Arndt et al., 2001; Thorne and Trendall, 2001). The Fortescue Group lavas originated from plume-generated komatiite volcanism that was contaminated by older crustal basement, in a similar way to Phanerozoic large igneous provinces (Mole et al., 2018).

3. Methods

Analyses were performed on powder aliquots from 2-3 kg of rock sample grounded in an agate mill. For Ce, Nd, and Hf measurements, 120-1200 mg of sample powder were digested in Parr© bombs. For Sm/Nd and Lu/Hf measurements, mixed ^{149}Sm-^{150}Nd and ^{176}Lu-^{180}Hf isotope tracers were added prior to digestion following previously described protocols (Münker et al., 2001; Hoffmann et al., 2011a). For La-Ce (ID) measurements, a 20% aliquot was spiked with a ^{138}La-^{142}Ce isotope tracer after sample digestion. For isotope analysis we additionally added 1 ml of 65% $HClO_4$ to some replicates after Parr© bomb digestions to prevent the formation of insoluble rare-earth elements (REE) and high field strength (HFSE)-fluorides although addition of $HClO_4$ did not have an effect on the results of concentration or isotope measurements (supplementary information S1). Lutetium-Hf separation was performed following the analytical protocol of Münker et al. (2001). The light rare-earth element (LREE)-bearing matrix from Lu-Hf separation as well as the 20% La-Ce ID aliquot were processed after

Schnabel et al. (2017). The leftover REE cut was then processed through Ln Spec resin after Pin and Zalduegui (1997) to obtain pure Sm and Nd fractions. Total procedural blanks were always <150 pg for Ce, <100 pg for La, <39 pg for Nd, <19 pg for Sm, and <140 pg for Hf and Lu, respectively, and were all negligible.

All ID and isotope composition measurements were performed on a Thermo Fischer Neptune© or a Thermo Fischer Neptune Plus© MC-ICP MS at Cologne. Lanthanum-Ce measurements were performed following the protocol of Schnabel et al. (2017), but for Ce isotope composition measurements, $10^{12}\Omega$ amplifiers were replaced by $10^{13}\Omega$ amplifiers. Mass bias correction was performed by using the exponential law and a ^{136}Ce/^{140}Ce=0.002124072 (Makishima and Nakamura, 1991). All Ce data are reported relative to the Mainz-AMES standard solution (^{138}Ce/^{136}Ce=1.33738) (Willbold, 2007). The tailing effect of ^{140}Ce on ^{136}Ce and ^{138}Ce was recorded by measuring the ratios of half-masses relative to the peak mass (Willbold, 2007), but tail contributions on ^{138}Ce were always in the sub-ppm range (e.g., Schnabel et al., 2017). For Ce ID measurements, Ba was used for mass bias correction assuming a ^{137}Ba/^{135}Ba ratio of 1.70383, whereas for La ID measurements, Nd was used for mass bias correction (^{146}Nd/^{144}Nd=0.7219). The external reproducibility for ^{138}Ce/^{136}Ce ratios is given as relative standard deviation (RSD) and amounts to ±21 ppm (2 RSD), based on multiple measurements (n=13) of six digestions of the reference material BHVO-2.

Neodymium isotope compositions are reported relative to a ^{143}Nd/^{144}Nd value of 0.511859 for La Jolla standard. Mass bias correction followed the exponential law using a ^{146}Nd/^{142}Nd of 0.7219. The external long-term reproducibility of Nd isotope measurements amounts to ±40 ppm (2 RSD) (cf. Marien et al., 2019). Hafnium isotope compositions are given relative to the Münster AMES standard, having a ^{176}Hf/^{177}Hf ratio of 0.282160 (Münker et al., 2001). All measured ^{176}Hf/^{177}Hf isotope data were mass bias corrected by using the exponential law and a ^{179}Hf/^{177}Hf of 0.7325. Mass bias correction for Lu measurements was performed by using a ^{173}Yb/^{171}Yb ratio of 1.29197. The external long-term reproducibility of ^{176}Hf/^{177}Hf analysis amounts to ±40 ppm (cf. Marien et al., 2019). The external reproducibilities on ^{138}La/^{136}Ce ^{147}Sm/^{144}Nd and ^{176}Lu/^{176}Hf amount to ≤0.2% (2 RSD).

Calculated errors on our reported initial Hf-Nd-Ce isotope compositions represent the propagated errors of the parent/daughter ratio, the age uncertainty and the external reproducibility given by multiple digestions of reference materials.

4. Results

4.1. Major and trace element compositions

Major and trace element data for mafic-ultramafic samples of the ~3.53-3.31 Ga Warrawoona and Kelly groups are broadly consistent with previously reported data for rocks from the EPT (Smithies et al., 2007a; Smithies et al., 2018). For mafic-ultramafic samples, MgO contents generally vary between 4.11-29.2 wt.% (Fig. 2) (see Tusch et al. (2020) for further information on major and trace element data). The concentrations of SiO_2 (43.7-54.1 wt.%), TiO_2 (0.218-2.00), and Al_2O_3 (4.88-14.9 wt.%) also vary significantly (Fig. 2). Primitive mantle normalized trace element patterns of these samples are predominantly flat, as indicated by moderate La/Yb_{CN} (0.546-3.32) and Gd/Yb_{PM} ratios (0.851-1.93) (Fig. 3). Some mafic samples show minor depletions of Nb and Ta compared to La (Nb/La=0.568-1.14) (Fig. 3). Ratios of Th/Yb are often lower (0.0535-0.697) when compared to previously published data for EPT samples (Smithies et al., 2018). In most samples, Ce anomalies are absent (Ce/Ce*=0.917-1.17), whereas Eu anomalies occur more frequently and range from 0.754-1.59.

The younger (c. 3.2 Ga) samples of the Soanesville Group, Dalton Suite, and Roebourne Group show similar MgO (6.84-25.7 wt.%), Al_2O_3 (2.44-10.2 wt.%) and SiO_2 contents (40.0-51.4 wt.%) compared to the older Warrawoona and Kelly Group samples, but exhibit significantly lower TiO_2 contents (0.170-0.656 wt.%) (Fig. 2). Furthermore, these samples show depletions of LREE over heavy rare-earth elements (HREE), as indicated by lower La/Yb_{CN} (0.761-4.27), and predominantly superchondritic Sm/Nd ratios (0.229-0.372) as previously described (Smithies et al., 2007a, 2018). Compared to the older Warrawoona and Kelly Group samples, Th/Yb (0.0834-0.229) are lower, Nb/La ratios define a narrower range (0.464-0.738), and Eu and Ce anomalies are largely absent (Ce/Ce*=0.962-0.990; Eu/Eu*=0.963-1.27).

Samples of the ~3.12-2.63 Ga Whundo Group, De Grey Supergroup, and the Fortescue Group show generally the highest SiO_2 (48.8-56.7 wt.%) and Al_2O_3 (9.29-15.6 wt.%) contents and the lowest MgO (5.29-15.6 wt.%), excluding two ultramafic rocks from the De Grey Supergroup (MgO>30 wt.%) (Fig. 2). Samples of the De Grey Supergroup have the highest incompatible trace element concentrations, including substantial LREE enrichments relative to HREE (La/Yb_{CN}=3.21-4.53) (Fig. 3). Significant depletions of Nb-Ta compared to La are present in most of these lithostratigraphic units (Nb/La=0.246-0.823), although the most pronounced and uniform Nb-Ta anomalies are found in the basalts and komatiites of the De Grey Supergroup (Nb/La=0.246-0.339). The oldest (~2.78 Ga) Fortescue Group samples are also characterized by low Nb/La ratios (0.29-0.36) and incompatible trace element patterns that are enriched in more incompatible trace elements (La/Yb_{CN}=1.09-9.19). These samples stand in marked contrast to the youngest (~2.63 Ga) Fortescue Group samples (Jeerinah Formation) that have predominantly flat primitive mantle normalized incompatible trace element patterns (La/Yb_{CN}=1.2-8.9) (Fig. 3).

4.2. Radiogenic isotopes

A total of 63 samples were analyzed for their ^{176}Lu-^{176}Hf and ^{147}Sm-^{143}Nd isotope compositions and a subset of 40 samples were analyzed for their ^{138}La-^{138}Ce isotope compositions (supplementary information S1). Age-corrected $\varepsilon Hf_{(i)}$ and $\varepsilon Nd_{(i)}$ values were normalized to the CHUR value of Bouvier et al. (2008) and $\varepsilon Ce_{(i)}$ values were normalized to the CHUR value of Willig and Stracke (2019) and Israel et al., (2019), giving combined $^{138}La/^{136}Ce$ and $^{138}Ce/^{136}Ce$ ratios of 0.1865 and 1.336878, respectively.

Initial $\varepsilon Hf_{(i)}$ values of EPT basalts range from 0.0 to +4.2 (excluding sample Pil16-24 having an $\varepsilon Hf_{(i)}$ value of +7.4), whereas komatiites tend to have higher $\varepsilon Hf_{(i)}$ values (+1.5 to +8.1; see Supplementary information S2), in accordance with previous observations by Nebel et al. (2014). Notably, negative $\varepsilon Hf_{(i)}$ and $\varepsilon Nd_{(i)}$ values were only found in the youngest samples (De Grey Supergroup and Fortescue Group; $\varepsilon Hf_{(i)}$=-2.7 to +5.0; $\varepsilon Nd_{(i)}$=-2.8 to + 3.2). Felsic to intermediate granitic samples of various age yield diverse $\varepsilon Hf_{(i)}$ values (-5.8 to +2.0) and $\varepsilon Nd_{(i)}$ values (-6.3 to +1.3) that are in good agreement with previously reported zircon data (e.g., Kemp et al., 2015; Gardiner et al., 2017; Petersson et al., 2019).

The majority of our samples display negative initial $\varepsilon Ce_{(i)}$ values. Samples without Ce/Ce* anomalies (Fig. 4) yield a narrow range in initial $\varepsilon Ce_{(i)}$ values (-0.4 to +0.61), whereas samples with Ce/Ce* anomalies show a significantly higher scatter in $\varepsilon Ce_{(i)}$ values (-7.4 to + 2.3). Generally, all three isotope systems show the same trends between 3.53 Ga and 2.63 Ga, where $\varepsilon Hf_{(i)}$ and $\varepsilon Nd_{(i)}$ broadly increase between 3.5-3.2 Ga, although the majority of 3.34 Ga basalt samples of the Kelly Group deviate towards slightly more unradiogenic values (Fig. 5). Cerium isotopes show a complementary trend, with decreasing $\varepsilon Ce_{(i)}$ values between 3.5-3.2 Ga and a slight increase at 3.34 Ga. Between ca. 2.9-2.7 Ga, $\varepsilon Hf_{(i)}$ and $\varepsilon Nd_{(i)}$ decrease sharply, while $\varepsilon Ce_{(i)}$ values increase slightly. The 2.63 Ga Jeerinah Formation deviates from that trend by showing significantly higher $\varepsilon Hf_{(i)}$ and $\varepsilon Nd_{(i)}$, as well as lower $\varepsilon Ce_{(i)}$ values.

5. Discussion

5.1. Alteration and its effects on radiogenic isotope systematics

Rocks from the Pilbara Craton have experienced a complex geological history, including hydrothermal alteration and metamorphism that subsequently modified the pristine geochemistry of these rocks (Collins and Van Kranendonk, 1999; Van Kranendonk et al., 2002). Thus, it is crucial to evaluate whether the samples analyzed in this study have preserved their primary REE and HFSE budgets. HFSE, Th, and REE display significant co-variations with Zr, indicating that these elements have not been substantially mobilized by secondary processes (Fig. 2) (see also Polat et al., 2002). Cerium anomalies in mafic samples are always smaller than 5% (excluding sample Pil16-44a: Ce/Ce*=1.2 and sample 179757: Ce/Ce*=0.92), indicating that the LREE were not substantially mobilized during secondary geological events (Fig. 4a) (Polat et al., 2002). Similar to previous studies on Archean rocks (e.g. Vervoort and Blichert-Toft, 1999; Nebel et al., 2014), initial $\varepsilon Hf_{(i)}$ and $\varepsilon Nd_{(i)}$ values (and also $\varepsilon Ce_{(i)}$ values) show a coherent evolution through time (Fig. 5). Furthermore, there are no co-variations between $\varepsilon Hf_{(i)}$, $\varepsilon Nd_{(i)}$, and $\varepsilon Ce_{(i)}$ and loss on ignition (LOI) and all three parent/daughter ratios correlate with each other, indicating primary magmatic trends (Figs. 4b and 4c). In contrast, all large ion lithophile elements were mobile during post-magmatic events, as suggested by poor correlations with Zr (Fig. 2f).

In marked contrast to the mafic rocks, most granitoids display negative Ce/Ce^* anomalies, as low as 0.835, that increase with increasing SiO_2 (Fig. 4a). This is surprising, as the granitoids studied have preserved a seemingly pristine mineralogy and have very low LOIs (<1.5 wt %). The Ce/Ce^* anomalies imply that the granitoids are prone to disturbance of the ^{138}La-^{138}Ce system, likely during oxidative weathering, where Ce^{4+} can become decoupled from the other REE^{3+}. We speculate that altered mafic volcanic rocks are less susceptible to terrestrial weathering than granites, as the mafic volcanics contain high amounts of secondary minerals (e.g., chlorite serpentine, epidote and amphibole) that might be more robust during oxidative terrestrial weathering.

The coupled behavior of $\varepsilon Hf_{(i)}$, $\varepsilon Nd_{(i)}$, and $\varepsilon Ce_{(i)}$ in mafic-ultramafic Pilbara rocks (Fig. 5) also argues against secondary alteration effects, as the three studied radioactive decay systematics should be variably affected by secondary alteration (e.g., Polat et al., 2002). Most importantly, all whole rock ^{147}Sm-^{143}Nd and ^{176}Lu-^{176}Hf (and ^{138}La-^{138}Ce) age regression lines for individual units yield ages which overlap within error with the reported stratigraphic ages for the formations from which they were sampled (Supplementary Figs. 1-3). Thus, we conclude that the initial Hf-Nd-Ce isotope compositions determined in this study are sufficiently robust to constrain the depletion history of the Archean mantle beneath the Pilbara Craton, although ^{138}La-^{138}Ce data for samples with Ce/Ce* anomalies are regarded as altered.

5.2. Effects of crustal contamination

Crustal contamination can strongly affect radiogenic isotope compositions and consequently obscure the information on parental mantle sources. The oldest mafic-ultramafic samples in our study (3.53-3.18 Ga) show a broad range of $\varepsilon Hf_{(i)}$ and $\varepsilon Nd_{(i)}$, correlating with La/Yb (Fig. 6f) but not with Nb/Th (Fig. 6d). This implies that the magmatic source mixed with a second isotopically heterogeneous component, but this was unlikely continental crust as it has characteristically low Nb/Th ratios. Similar co-variations are also expected for Ce isotopes, but such changes are not easily analytically resolvable. As most of the 3.53-3.18 Ga mafic samples also fall on the MORB-OIB array in Th/Yb vs. Nb/Yb space (Fig. 6a), it seems more plausible that the two components involved were primitive mantle-like source and a more depleted mantle endmember.

Unlike the older mafic samples, younger units (De Grey Supergroup, Fortescue Group, and potentially the Whundo Group) show decreasing Nb/Th with decreasing $\varepsilon Hf_{(i)}$ (Fig. 6c). This observation is best explained by the interaction of primary melts with an enriched component, likely continental crust(Arndt et al., 2001; Mole et al., 2018), but possibly also mantle source enrichment (Smithies et al., 2005a).

5.3. Cerium isotope constraints

Although the ^{138}La-^{138}Ce system has so far only rarely been applied in geochemistry, it can put additional constraints on the implications that are drawn from combined ^{176}Lu-^{176}Hf and ^{147}Sm-^{143}Nd systematics, e.g. the origin of strongly decoupled Hf and Nd isotope compositions found in Archean mafic rock successions (Vervoort and Blichert-Toft, 1999; Vervoort et al., 2000; Hoffmann et al., 2011b). One process that was inferred for this decoupling is the fractionation of Ca-perovskite during magma ocean crystallization (e.g. Hoffmann et al., 2011b; Rizo et al., 2011). In the presence of perovskite, LREE can be strongly fractionated from Lu and Hf (Corgne and Wood, 2002; Corgne et al., 2005). In the lower mantle, the LREE are mainly affected by the fractionation of Ca- and Mg-perovskite that have $D_{La}<D_{Ce}$ and $D_{Sm}>D_{Nd}$, causing pervoskite cumulates to have superchondritic Sm/Nd ratios but subchondritic La/Ce ratios (Fig. 4c). Although Ca-perovskite is less abundant than Mg-perovskite, all the LREE are significantly more compatible in the former ($D_{LREE}>1$) than the latter phase ($D_{LREE}<1$). Lutetium and Hf show the opposite behavior during perovskite fractionation with D_{Lu}/D_{Hf} ~0.5 for Mg-perovskite, and D_{Lu}/D_{Hf} ratio of >5 for Ca-perovskite (Corgne and Wood, 2002; Corgne et al., 2005). Consequently, early segregation of Ca- and Mg-perovskite would produce perovskite cumulates that exhibit lower La/Ce and higher Sm/Nd ratios compared to bulk silicate Earth, whereas the Lu/Hf ratio is variable, and strongly dependent on the fractions of Ca- and Mg-perovskite being crystallized (e.g. Hoffmann et al., 2011b; Rizo et al., 2011; Puchtel et al., 2016). Thus, early Ca-Mg-perovskite cumulates would evolve towards negative εCe values, positive εNd values, and variable εHf values.

To further quantify this process, we conducted trace element modeling, assuming crystallization of 4.5% Ca-perovskite, 85% Mg-perovskite, and 10.5% ferropericlase, in accord with previous estimates (e.g. Hoffmann et al., 2011b; Puchtel et al., 2016; Rizo et al., 2016) (see Supplementary information S2). Higher abundances of Ca-perovskite would generate extremely unradiogenic Hf isotope compositions over time, whereas lower Ca-perovskite abundances would result in extremely positive

Zr-Hf anomalies relative to REE. The age for the magma ocean crystallization was set to 4.4 Ga, although changing that age by ±100 Ma hardly affects the isotopic outcome at 3.5 Ga. Depending on the style of crystallization (fractional vs. equilibrium crystallization) and the fraction of crystallized melt (5% to 60%), perovskite cumulates in both crystallization modes develop towards positive εNd values (ca. +0.8 to +5.5), variable εHf values (-5.4 to +3.0), and strongly negative εCe values (-1.0 to -1.5) at 3.5 Ga. The εCe values of these modelled cumulates at 3.5 Ga would be significantly lower than εCe values of our oldest 3.53-3.34 Ga samples from the EPT (-0.3 to +0.3) (Fig. 5c). The exotic isotope composition that is derived from our model is unmatched by our observed data and thus precludes Ca-Mg perovskite cumulates to be a potential source for Pilbara rocks, which is furthermore consistent with relatively high ^{138}La/^{136}Ce ratios in our samples (Fig. 4c) and an insignificant fractionation of Zr-Hf from Sm-Nd (Fig. 3). Althogether, the geochemical evidence suggests that the decoupling of Hf-Nd isotopes in the Pilbara Craton does not stem from an early magma ocean crystallization event, but rather originates from early differentiation events in the upper mantle.

The combination of Ce, Nd and Hf isotopes provide a powerful tool to gain better insight into the history of the early Earth and demonstrate that Ca-Mg cumulate segregation during magma ocean crystallization can be discarded as a cause for extremely high εHf$_{(i)}$ values found in Archean rocks from the Pilbara Craton. It still remains ambiguous, however, if the decoupling of Hf and Nd isotopes in other Archean rocks can be explained by perovsite segregation (e.g., Hoffmann et al., 2011b; Puchtel et al., 2016; Rizo et al., 2016) or not (e.g., Hoffmann and Wilson, 2017), although future ^{138}La-^{138}Ce isotope studies might help to place better constraints on this issue.

5.4. Hafnium, Nd and Ce isotope systematics of Pilbara mafic-ultramafic rocks and their implications for mantle evolution

Some mafic-ultramafic rocks from the Pilbara Craton show a decoupling of their initial Hf-Nd-Ce isotope compositions, with extremely radiogenic $\varepsilon Hf_{(i)}$ values up to +8.1 at significantly lower $\varepsilon Nd_{(i)}$ values (Figs. 5a and 7b). These findings are in apparent contrast to the studies by Kemp et al. (2015) and Petersson et al., (2019; 2020) who postulated a near-chondritic mantle at ~3.6 Ga. Their studies focused on Hf isotope compositions measured in inherited and detrital zircons from granitoids and sedimentary rocks (Kemp et al., 2015) and zircons from mafic to felsic rock successions (Petersson et al., 2019; Petersson et al., 2020). However, zircons in granitoids may not reveal the full depletion history of the Archean mantle, and in particular the TTGs that are thought to result from remelting of older mafic protoliths (Smithies et al., 2009; Hoffmann et al., 2011a; Gardiner et al., 2017; Johnson et al., 2017). Depending on the time elapsed between mantle melting, formation of mafic proto-crust, and TTG formation (hereafter the crustal residence time), the mafic protolith may have developed unradiogenic Hf isotope compositions. Consequently, zircons that grew during TTG crystallization may have inherited their initial Hf isotope compositions from the evolved isotope composition of the mafic protolith rather than from the ambient mantle.

Petersson et al., (2019; 2020) reported chondrite-like Hf isotope compositions for 3.59-3.31 Ga zircons from mafic to intermediate rocks from the Pilbara Craton, from which they argued for a chondritic composition of the ambient mantle until ~3.6 Ga. However, the basalts of their study show significant LREE enrichment and strong Nb-Ta depletions. Based on our study, this is best explained by the interaction with an enriched component, most likely reflecting crustal contamination. This is also in accord with previous work by Smithies et al., (2018) who have found evidence for crustally contaminated ~3.5 Ga Pilbara basalts displaying similarly low Nb/Th ratios as those reported by Petersson et al., (2019). Moreover, the presence of basalts with near-chondritic $\varepsilon Hf_{(i)}$ does not exclude the presence of more depleted mantle, as shown by our study (Figs. 5-8). If such rocks are interpreted as crustally contaminated, as we favor, they rather provide evidence for the presence of ≥3.59 Ga felsic basement beneath the Pilbara Craton, which is consistent with inherited zircon data (Van Kranendonk et al., 2002).

Due to the predominantly positive $\varepsilon Hf_{(i)}$ and $\varepsilon Nd_{(i)}$ values in mafic-ultramafic rocks analyzed here, we conclude that the ambient mantle of the Pilbara Craton must have undergone older depletion events prior to 3.5 Ga, as suggested by previously studies (Gruau et al., 1987; Arndt et al., 2001; Smithies et al., 2007b; Tessalina et al., 2010; Nebel et al., 2014; Gardiner et al., 2017). Hafnium and Nd isotope compositions both suggest an onset of mantle-crust differentiation processes at ~4.2 Ga, evolving towards present day εHf and εNd values of +16 and +10, respectively. In contrast, Ce isotopes are not able to place further constraints on that depletion event due to somewhat smaller isotope variations, although Ce isotope evidence is still in accord with a ~4.2 Ga depletion event (assuming a present day εCe of the depleted upper mantle of -1.5). Nevertheless, there are some samples with near-chondritic $\varepsilon Hf_{(i)}$ and $\varepsilon Nd_{(i)}$ values that lack evidence for crustal contamination (Pil16-17, Pil16-20b). These samples likely originated from more primitive mantle sources, possibly from primitive upwelling mantle material added to the depleted upper mantle (cf. Bédard, 2018). Importantly, however, we observe an increase in $\varepsilon Hf_{(i)}$ and $\varepsilon Nd_{(i)}$ and a decrease in $\varepsilon Ce_{(i)}$ with decreasing crystallization age between 3.53 Ga and 3.12 Ga. This is best explained by a depleted mantle source that evolved through geologic time (*cf.* Smithies et al., 2005b).

Initial Hf and Nd isotope compositions in rocks from the slightly younger (~3.26-3.18 Ga) Roebourne Group, Soanesville Group and Dalton Suite that are all ascribed to a rift-related setting are significantly more radiogenic, with $\varepsilon Ce_{(i)}$ being more unradiogenic, if compared to samples of the 3.34 Ga old Kelly Group (Arndt et al., 2001; Smithies et al., 2007b; Van Kranendonk et al., 2010). In addition, the majority of samples from these younger successions are characterized by elevated Sm/Nd ratios and MORB-like trace element patterns, implying a more depleted mantle source compared to the plume-related rocks of the Warrawoona and Kelly groups, as previously postulated by Smithies et al. (2005b). The observed change in the trace element geochemistry is likely linked to a proposed change in geodynamic setting at ~3.2 Ga from upwelling/plume-like dominated processes to modern style plate tectonics (Smithies et al., 2005a; Smithies et al., 2005b; Van Kranendonk et al., 2007; Van Kranendonk et al., 2010). We conclude that this change from mantle upwelling/plume-related volcanism before ~3.2 Ga to rift-related volcanism after ~3.2 Ga (Smithies et al., 2005b; Van Kranendonk et al., 2010) is mirrored by a change in ambient mantle composition. Such a model is also in accord with observations of increasing PGE abundances (Maier et al., 2009) and decreasing ^{182}W isotope anomalies (Tusch et al., 2020) at the same time, which are suggested to mirror widespread homogenization of the mantle at this time by more efficient vertical mixing. The long-lived isotope systems analyzed in this study can help to better constrain how the involvement of different mantle reservoirs triggered homogenization of late veneer material. Between 3.5 and 3.2 Ga, deep-rooted upwelling mantle manterial that was not yet equilibrated with late veneer material mixed with shallower mantle regions that already equilibrated with late veneer material. Due to a change in the geodynamic setting at 3.2 Ga (Van Kranendonk et al., 2010), the supply in the upper mantle by upwelling mantle with pre-late veneer signature ceased, resulting in decreased $\mu^{182}W$ values (Tusch et al., 2020) and increased PGE concentrations (Maier et al., 2009) after ~3.2 Ga.

With the emergence of localized subduction by ~3.1 Ga, an arc-like setting led to formation of the 3.12 Ga Whundo Group (Krapez and Eisenlohr, 1998; Smithies et al., 2005a; Smithies et al., 2007c) . Our data for Whundo Group samples generally indicate the involvement of an enriched component as implied by somewhat lower Nb/Th ratios and $\varepsilon Hf_{(i)}$ and $\varepsilon Nd_{(i)}$ values in these samples (Figs. 3, 5, 6c). In the context of a subduction-like setting that was previously proposed for the Whundo Group (Krapez and Eisenlohr, 1998; Smithies et al., 2005a; Smithies et al., 2007c), it is possible that this enriched component originates from remelting a subducting crust. However, the small number of samples (n=3) analyzed from the Whundo Group hampers a more detailed interpretation of the tectonic setting of the Whundo Group. After the collision of the WPS and the EPT at 3.07 Ga, volcanics of the ~3.0 Ga De Grey Supergroup tapped a metasomatized mantle that was likely re-enriched within a subduction setting at ~3.12 Ga (Smithies et al., 2004; Smithies et al., 2005a). This is mirrored by significantly lower $\varepsilon Hf_{(i)}$ and $\varepsilon Nd_{(i)}$ and higher $\varepsilon Ce_{(i)}$ values in all of the rocks of the De Grey Supergroup (Fig. 5). The absence of samples that have positive $\varepsilon Hf_{(i)}$, $\varepsilon Nd_{(i)}$ and lower $\varepsilon Ce_{(i)}$

values argues against a role of AFC processes and supports evidence that the enriched component must have already been distributed within the mantle source (Smithies et al., 2004).

The older units (2.78-2.63 Ga) of the Fortescue Group were contaminated by significantly older crust, as indicated by AFC processes becoming apparent from strongly negative $\varepsilon Hf_{(i)}$ and $\varepsilon Nd_{(i)}$ and positive $\varepsilon Ce_{(i)}$ values that are found in some samples of the Fortescue Group (Arndt et al., 2001; Smithies et al., 2007b; Mole et al., 2018). In contrast, the majority of the younger ~2.63 Ga Jeerinah Formation within the Fortescue Group show no evidence for crustal contamination (except possibly sample 201476), by generally having elevated $\varepsilon Hf_{(i)}$ (+4.2 to +5.0) and $\varepsilon Nd_{(i)}$ (+0.5 to +3.2), and low $\varepsilon Ce_{(i)}$ values (-0.44 to -1.3), suggesting an origin from a depleted mantle domain.

5.5. A genetic model for the evolution of the East Pilbara Terrane

Our Hf and Nd isotope results reveal distinct differences between most komatiites and basalts. As $\varepsilon Hf_{(i)}$ values are significantly higher in komatiites compared to most basalts, different mantle reservoirs must have been involved in the formation of the Pilbara Craton. Furthermore, the majority of basalts from the Warrawoona Group have $\varepsilon Hf_{(i)}$ and $\varepsilon Nd_{(i)}$ values that are best explained by an origin from a shallow, depleted upper mantle domain (Gruau et al., 1987; Nisbet et al., 1993; Arndt et al., 2001; Smithies et al., 2005b; Smithies et al., 2007b; Sossi et al., 2016; Bédard, 2018). Nevertheless, some samples investigated here show near-chondritic $\varepsilon Hf_{(i)}$, $\varepsilon Nd_{(i)}$ and $\varepsilon Ce_{(i)}$ values that cannot be explained by crustal contamination. This observation rather implies near-primitive mantle sources for at least some rocks from the Pilbara Craton that likely represent material from deep-rooted upwelling mantle (see also Van Kranendonk et al., 2007a, 2015). However, it is still ambiguous whether komatiites in general were formed in a plume setting (e.g., Arndt et al., 1997; Arndt et al., 2001; Smithies et al., 2005b) or as a consequence of mantle overturn events (e.g., Bédard, 2018). As our model can be applied to both scenarios, we refer to this process as '*upwelling mantle*' without preferring any of these two processes.

Interestingly, two Warrawoona Group samples (Pil16-17 and Pil16-20b) of this study that display chondritic Hf-Nd-Ce isotope compositions were melted in deeper parts of the mantle, as indicated by the highest Gd/Yb_{PM}=1.72-1.93 and TiO_2/Yb=0.752-0.738. Pressure and temperature estimates following the approach of Lee et al. (2009) confirm that sample Pil16-20b was melted at P-T conditions exceeding the estimates for all other Warrawoona Group samples from the Pilbara Craton by at least 3 GPa and 150°C (Supplementary Fig. 4; sample Pil16-17 could not be calculated). In contrast, all other Warrawoona Group samples with more radiogenic $\varepsilon Hf_{(i)}$ and $\varepsilon Nd_{(i)}$ values were melted in shallower mantle regions as indicated by near-chondritic Gd/Yb_{PM}. As the Paleoarchean basalts from this study show a continuous spectrum from near-chondritic to increasingly positive $\varepsilon Hf_{(i)}$ and $\varepsilon Nd_{(i)}$ values expected for depleted mantle at that time, we conclude that a upper depleted mantle endmember was mixed with a near-chondritic upwelling mantle between 3.53-3.34 Ga (Figs. 5-8).

In contrast to the majority of the basalts analyzed here, most komatiitic rocks and one basalt from the EPT show highly radiogenic initial Hf isotope compositions that are decoupled from their Nd-Ce isotope compositions. This decoupling can be explained by older melt loss from garnet-bearing residual mantle reservoirs that can efficiently fractionate Lu/Hf from Sm/Nd and La/Ce.

In order to reconcile our observations, we conducted isotope and trace element modelling to explain the decoupled Hf-Nd-Ce isotope compositions, as well as the trace element characteristics of rocks from the Pilbara Craton. Following Sossi et al. (2016), a non-modal batch melting model was used. The first step comprised extraction of 10% melt from a lherzolite in the garnet stability field at 4.2 Ga, forming residual mantle domains. We have chosen this age based on our data, as it likely reflects the onset of mantle-crust differentiation beneath the Pilbara Craton (Fig. 5). Within 700 Ma, such isolated residual mantle domains may have evolved towards extreme $\varepsilon Hf_{(i)}$ $\varepsilon Nd_{(i)}$ and $\varepsilon Ce_{(i)}$ values of +42, +16 and -1.2, respectively, in accord with present day observations from abyssal peridotites (Salters et al., 2011). Due to the refractory nature of such depleted mantle domains, higher melting temperatures are required, which can explain why the decoupling of Hf-Nd-Ce isotope compositions is mainly found in komatiites as they are a product of high temperature mantle melting (e.g., Arndt et al., 1997). This model can also explain the highly radiogenic but coupled Hf and Nd isotope compositions of sample 179757, where the residual mantle contains more clinopyroxene than orthopyroxene (see Supplementary information S3). Mass balance calculations, as illustrated in Supplementary Figure 5, suggest that in-mixing of more fertile primitive mantle material would efficiently dilute the Hf-Nd-Ce isotope compositions of such residual domains. Our model demonstrates that mixing between primitive mantle with Hadean residual mantle at almost equal proportions (30-50% residual mantle and 50-70% primitive mantle) creates a hybrid mantle source with trace element and Hf-Nd-Ce isotope characteristics that match those observed in rocks from the Pilbara Craton (Fig. 7, Supplementary Fig. 5).

Unfractionated Gd/Yb_{PM}=0.851-1.25 and relatively low TiO_2/Yb ratios of all EPT komatiites suggest melting within the spinel stability field, in accord with P-T estimates for the Warrawoona Group (Lee et al., 2009) (Supplementary Fig. 4). This apparent contrast to our proposed residual mantle domains from the garnet stability field can be explained by two processes: (1) Anomalously high temperatures of the upwelling mantle shifted the spinel stability field towards significantly higher depths (e.g., Klemme et al., 2009); or (2) convective transport of the residual mantle domains to shallower depths outside the garnet stability field, as previously proposed for the 3.33 Ga Commondale komatiite suite in South Africa (Hoffmann and Wilson, 2017 and refs. therein). As previously observed by Nebel et al. (2014), and confirmed here, the extremely radiogenic $\varepsilon Hf_{(i)}$ values in Pilbara komatiites are absent after ~3.2 Ga (Fig. 5), consistent with the proposed change in plate tectonic regime recorded in the Pilbara Craton. As the onset of Phanerozoic-style plate tectonics has long been interpreted to result from decreasing mantle temperatures (cf. Davies, 1992), we therefore conclude that it was this factor, more than any other, that reduced the proportions of residual mantle domains tapped by mantle melts after 3.2 Ga.

6. Conclusions

A combined Hf-Nd-Ce isotope dataset for mafic-ultramafic rocks from the Pilbara Craton, covering all major stratigraphic units, places new constraints on the geodynamic evolution of the Pilbara Craton and the early Archean mantle in general. In mafic-ultramafic successions of the Pilbara Craton, these isotope systematics were insignificantly affected by post-magmatic alteration, implying that the decoupling of Hf isotopes from Nd-Ce isotopes is a primary magmatic feature. Consistently elevated Nb/La ratios in all samples >3.2 Ga preclude AFC processes to have operated during their formation, possibly reflecting the limited extent of evolved continental crust in the Pilbara Craton during the early Archean.

Perovskite fractionation in an ancient magma ocean cannot explain the observed variability in Hf-Nd-Ce isotope compositions, and the Ce-Nd array of the accessible upper mantle was near-chondritic by early Archean time. Rather, the broad variety of $\varepsilon Hf_{(i)}$, $\varepsilon Nd_{(i)}$ and $\varepsilon Ce_{(i)}$ values imply that at least two distinct mantle reservoirs were involved in the formation of these rocks. One reservoir, most likely ambient upper mantle, must have had a long depletion history, commencing at ~4.2 Ga, as constrained by the most depleted basalt samples. A second reservoir with near-chondritic radiogenic isotope ratios likely tapped the lower mantle by continuous mantle upwelling. Most komatiites have significantly higher $\varepsilon Hf_{(i)}$ values that are decoupled from Nd-Ce compositions. This is likely explained by high temperature melting of residual mantle domains that have experienced a previous melt depletion history in the garnet stability field.

Samples younger than 3.2 Ga exhibit significantly lower Nb/La ratios and, in some cases, unradiogenic Hf and Nd isotope compositions, reflecting the involvement of enriched components via subduction zone recycling and crustal contamination. Collectively, our study demonstrates that the radiogenic isotope composition of mafic-ultramafic rocks from Pilbara Craton provides an unprecedented insight into mantle depletion history, further illustrating that depletion of the mantle may have commenced relatively early in Earth's history, in late Hadean time.

Acknowledgements

E.H and C.M. acknowledge funding through the European Commission by ERC grant 669666 'Infant Earth'. F. Wombacher, and A. Katzemich and other laboratory support staff are thanked for their support in the Lab. S. Kommescher is thanked for helpful discussions. H. Smithies and H. Howard publish with the permission of the Executive Director of the Geological Survey of Western Australia. We thank Nicholas Gardiner and Oliver Nebel for constructive reviews that helped to improve the manuscript and we also thank Frederic Moynier for editorial handling.

References

Arndt N., Bruzak G. and Reischmann T. (2001) The oldest continental and oceanic plateaus: geochemistry of basalts and komatiites of the Pilbara Craton, Australia. In: *Ernst, R.E., Buchan, K.L. (Eds.), Mantle Plumes Their Identif. Through Time,* **352**, 359–387.

Arndt N. T., Kerr A. C. and Tarney J. (1997) Dynamic melting in plume heads: the formation of Gorgona komatiites and basalts. *Earth Planet. Sci. Lett.* **146**, 289–301. Available at: http://orca.cf.ac.uk/9575/%5Cnhttp://linkinghub.elsevier.com/retrieve/pii/S0012821X96002191.

Bédard J. H. (2018) Stagnant lids and mantle overturns: Implications for Archaean tectonics, magmagenesis, crustal growth, mantle evolution, and the start of plate tectonics. *Geosci. Front.* **9**, 19–49. Available at: https://doi.org/10.1016/j.gsf.2017.01.005.

Bennett V. C., Nutman A. P. and McCulloch M. T. (1993) Nd isotopic evidence for transient, highly depleted mantle reservoirs in the early history of the Earth. *Earth Planet. Sci. Lett.* **119**, 299–317.

Bouvier A., Vervoort J. D. and Patchett P. J. (2008) The Lu-Hf and Sm-Nd isotopic composition of CHUR: Constraints from unequilibrated chondrites and implications for the bulk composition of terrestrial planets. *Earth Planet. Sci. Lett.* **273**, 48–57.

Collins W. J. and Van Kranendonk M. J. (1999) Model for the development of kyanite during partial convective overturn of Archean granite-greenstone terranes: The Pilbara Craton, Australia. *J. Metamorph. Geol.* **17**, 145–156.

Corgne A., Liebske C., Wood B. J., Rubie D. C. and Frost D. J. (2005) Silicate perovskite-melt partitioning of trace elements and geochemical signature of a deep perovskitic reservoir. *Geochim. Cosmochim. Acta* **69**, 485–496.

Corgne A. and Wood B. J. (2002) CaSiO3 and CaTiO3 perovskite-melt partitioning of trace elements: Implications for gross mantle differentiation. *Geophys. Res. Lett.* **29**, 39-1-39–4.

Davies G. F. (1992) On the emergence of plate tectonics. *Geology* **20**, 963–966.

Gardiner N. J., Hickman A. H., Kirkland C. L., Lu Y., Johnson T. and Zhao J. X. (2017) Processes of crust formation in the early Earth imaged through Hf isotopes from the East Pilbara Terrane. *Precambrian Res.* **297**, 56–76.

Gruau G., Jahn B. M., Glikson A. Y., Davy R., Hickman A. H. and Chauvel C. (1987) Age of the Archean Talga-Talga Subgroup, Pilbara Block, Western Australia, and early evolution of the mantle: new SmNd isotopic evidence. *Earth Planet. Sci. Lett.* **85**, 105–116.

Gruau G., Rosing M., Bridgwater D. and Gill R. C. O. (1996) Resetting of Sm-Nd systematics during metamorphism of > 3.7-Ga rocks: Implications for isotopic models of early Earth differentiation. *Chem. Geol.* **133**, 225–240.

Hickman A. H. (2012) Review of the Pilbara Craton and Fortescue Basin, Western Australia: Crustal evolution providing environments for early life. *Isl. Arc* **21**, 1–31.

Hoffmann J. E., Münker C., Næraa T., Rosing M. T., Herwartz D., Garbe-Schönberg D. and Svahnberg H. (2011a) Mechanisms of Archean crust formation inferred from high-precision HFSE systematics in TTGs. *Geochim. Cosmochim. Acta* **75**, 4157–4178.

Hoffmann J. E., Münker C., Polat A., Rosing M. T. and Schulz T. (2011b) The origin of decoupled Hf-Nd isotope compositions in Eoarchean rocks from southern West Greenland. *Geochim. Cosmochim. Acta* **75**, 6610–6628.

Hoffmann J. E. and Wilson A. H. (2017) The origin of highly radiogenic Hf isotope compositions in 3.33 Ga Commondale komatiite lavas (South Africa). *Chem. Geol.* **455**, 6–21. Available at: http://dx.doi.org/10.1016/j.chemgeo.2016.10.010.

Israel C., Boyet M., Doucelance R., Bonnand P., Frossard P., Auclair D. and Bouvier A. (2019) Formation of the Ce-Nd mantle array: Crustal extraction vs. recycling by subduction. *Earth Planet. Sci. Lett.* **1**, 1–12. Available at: https://linkinghub.elsevier.com/retrieve/pii/S0012821X19306338.

Johnson T. E., Brown M., Gardiner N. J., Kirkland C. L. and Smithies R. H. (2017) Earth's first stable continents did not form by subduction. *Nature* **543**, 239–242.

Kemp A. I., Hickman A. H. and Kirkland C. L. (2015) Report 151: Early Evolution of the Pilbara Craton from Hf isotopes in detrital and inherited zircons. *Precambrian Res.* **261**, 26.

Klemme S., Ivanic T. J., Connolly J. A. D. and Harte B. (2009) Thermodynamic modelling of Cr-bearing garnets with implications for diamond inclusions and peridotite xenoliths. *Lithos* **112**, 986–991. Available at: http://dx.doi.org/10.1016/j.lithos.2009.05.007.

Krapez B. and Eisenlohr B. (1998) Tectonic settings of Archaean (3325-2775 Ma) crustal-supracrustal belts in the West Pilbara Block. *Precambrian Res.* **88**, 173–205.

Lee C. T. A., Luffi P., Plank T., Dalton H. and Leeman W. P. (2009) Constraints on the depths and temperatures of basaltic magma generation on Earth and other terrestrial planets using new thermobarometers for mafic magmas. *Earth Planet. Sci. Lett.* **279**, 20–33.

Maier W. D., Barnes Stephen J., Campbell I. H., Fiorentini M. L., Peltonen P., Barnes Sarah Jane and Smithies R. H. (2009) Progressive mixing of meteoritic veneer into the early Earths deep mantle. *Nature* **460**, 620–623.

Makishima A. and Nakamura E. (1991) Precise measurement of cerium isotope composition in rock samples. *Chem. Geol.* **94**, 1–11. Available at: http://dx.doi.org/10.1016/S0009-2541(10)80012-9.

Marien C. S., Hoffmann J. E., Garbe-Schönberg C. D. and Münker C. (2019) Petrogenesis of plagiogranites from the Troodos Ophiolite Complex, Cyprus. *Contrib. to Mineral. Petrol.* **174**, 1–24. Available at: https://doi.org/10.1007/s00410-019-1569-3.

Mole D. R., Barnes S. J., Yao Z., White A. J. R., Maas R. and Kirkland C. L. (2018) The Archean Fortescue large igneous province: A result of komatiite contamination by a distinct Eo-Paleoarchean crust. *Precambrian Res.* **310**, 365–390.

Münker C., Weyer S., Scherer E. and Mezger K. (2001) Seperation of high field strength elements (Nb, Ta, Zr, Hf) and Lu from rock samples for MC-IPMS measurements. *Geochemistry Geophys. Geosystems* **2**, 1–19.

Nebel O., Arculus R. J., Ivanic T. J. and Nebel-Jacobsen Y. J. (2013) Lu-Hf isotopic memory of plume-lithosphere interaction in the source of layered mafic intrusions, Windimurra Igneous Complex, Yilgarn Craton, Australia. *Earth Planet. Sci. Lett.* **380**, 151–161. Available at: http://dx.doi.org/10.1016/j.epsl.2013.08.019.

Nebel O., Campbell I. H., Sossi P. A. and Van Kranendonk M. J. (2014) Hafnium and iron isotopes in early Archean komatiites record a plume-driven convection cycle in the Hadean Earth. *Earth Planet. Sci. Lett.* **397**, 111–120. Available at: http://dx.doi.org/10.1016/j.epsl.2014.04.028.

Nisbet E. G., Cheadle M. J., Arndt N. T. and Bickle M. J. (1993) Constraining the potential temperature of the Archaean mantle: A review of the evidence from komatiites. *Lithos* **30**, 291–307.

Petersson A., Kemp A. I. S., Gray C. M. and Whitehouse M. J. (2020) Formation of early Archean Granite-Greenstone Terranes from a globally chondritic mantle: Insights from igneous rocks of the Pilbara Craton, Western Australia. *Chem. Geol.* **551**.

Petersson A., Kemp A. I. S., Hickman A. H., Whitehouse M. J., Martin L. and Gray C. M. (2019) A new 3.59 Ga magmatic suite and a chondritic source to the east Pilbara Craton. *Chem. Geol.* **511**, 51–70. Available at: https://doi.org/10.1016/j.chemgeo.2019.01.021.

Pin C. and Zalduegui J. (1997) Sequential separation of light rare-earth elements, thorium and uranium by miniatureized extraction chromatography: applicaiton to isotopic analyses of silicate rocks. *Anal. Chim. Acta* **229**, 79–89.

Polat A., Hofmann A. W. and Rosing M. T. (2002) Boninite-like volcanic rocks in the 3.7 – 3.8 Ga Isua greenstone belt , West Greenland : geochemical evidence for intra-oceanic subduction zone processes in the early Earth. *Chem. Geol.* **184**, 231–254.

Puchtel I. S., Blichert-Toft J., Touboul M., Horan M. F. and Walker R. J. (2016) The coupled 182W-142Nd record of early terrestrial mantle differentiation Igor. *Geochemistry Geophys. Geosystems* **17**, 1312–1338.

Rizo H., Boyet M., Blichert-Toft J. and Rosing M. (2011) Combined Nd and Hf isotope evidence for deep-seated source of Isua lavas. *Earth Planet. Sci. Lett.* **312**, 267–279. Available at: http://dx.doi.org/10.1016/j.epsl.2011.10.014.

Rizo H., Walker R. J., Carlson R. W., Touboul M., Horan M. F., Puchtel I. S., Boyet M. and Rosing M. T. (2016) Early Earth differentiation investigated through 142Nd, 182W, and highly siderophile element abundances in samples from Isua, Greenland. *Geochim. Cosmochim. Acta* **175**, 319–336. Available at: http://dx.doi.org/10.1016/j.gca.2015.12.007.

Salters V. J. M., Mallick S., Hart S. R., Langmuir C. E. and Stracke A. (2011) Domains of depleted mantle: New evidence from hafnium and neodymium isotopes. *Geochemistry, Geophys. Geosystems* **12**, 1–18.

Schnabel C., Muenker C. and Strub E. (2017) La-Ce isotope measurements by Multicollector-ICPMS. *J. Anal. At. Spectrom.* **32**, 2360–2370. Available at: http://pubs.rsc.org/en/Content/ArticleLanding/2017/JA/C7JA00256D.

Smithies R. H., Champion D. C. and Van Kranendonk M. J. (2007a) Chapter 4.2 The Oldest Well-Preserved Felsic Volcanic Rocks on Earth: Geochemical Clues to the Early Evolution of the Pilbara Supergroup and Implications for the Growth of a Paleoarchean Protocontinent. *Dev. Precambrian Geol.* **15**, 339–367.

Smithies R. H., Champion D. C. and Van Kranendonk M. J. (2009) Formation of Paleoarchean continental crust through infracrustal melting of enriched basalt. *Earth Planet. Sci. Lett.* **281**, 298–306. Available at: http://dx.doi.org/10.1016/j.epsl.2009.03.003.

Smithies R. H., Champion D. C., Van Kranendonk M. J. and Hickman A. H. (2007b) GEOCHEMISTRY OF VOLCANIC ROCKS OF THE NORTHERN PILBARA CRATON WESTERN AUSTRALIA. *GSWA Rep. 104*, 48.

Smithies R. H., Champion D. C., Van Kranendonk M. J., Howard H. M. and Hickman A. H. (2005a) Modern-style subduction processes in the Mesoarchaean: Geochemical evidence from the 3.12 Ga Whundo intra-oceanic arc. *Earth Planet. Sci. Lett.* **231**, 221–237.

Smithies R. H., Champion D. C. and Sun S. S. (2004) Evidence for early LREE-enriched mantle source regions: Diverse magmas from the c. 3·0 Ga Mallina Basin, Pilbara Craton, NW Australia. *J. Petrol.* **45**, 1515–1537.

Smithies R. H., Ivanic T. J., Lowrey J. R., Morris P. A., Barnes S. J., Wyche S. and Lu Y.-J. (2018) Two distinct origins for Archean greenstone belts. *Earth Planet. Sci. Lett.* **487**, 106–116. Available at: http://linkinghub.elsevier.com/retrieve/pii/S0012821X18300529.

Smithies R. H., Van Kranendonk M. J. and Champion D. C. (2005b) It started with a plume - Early Archaean basaltic proto-continental crust. *Earth Planet. Sci. Lett.* **238**, 284–297.

Smithies R. H., Van Kranendonk M. J. and Champion D. C. (2007c) The Mesoarchean emergence of modern-style subduction. *Gondwana Res.* **11**, 50–68.

Sossi P. A., Eggins S. M., Nesbitt R. W., Nebel O., Hergt J. M., Campbell I. H., O'Neill H. S. C., Kranendonk M. Van and Rhodri Davies D. (2016) Petrogenesis and geochemistry of Archean Komatiites. *J. Petrol.* **57**, 147–184.

Tessalina S. G., Bourdon B., Van Kranendonk M., Birck J. L. and Philippot P. (2010) Influence of Hadean crust evident in basalts and cherts from the Pilbara Craton. *Nat. Geosci.* **3**, 214–217. Available at: http://dx.doi.org/10.1038/ngeo772.

Thorne A. M. and Trendall A. F. (2001) Geology of the Fortescue Group, Pilbara Craton, Western Australia. *Geol. Surv. West. Aust. Bull.* **144**, 1–249.

Tusch J., Münker C., Hasenstab E., Jansen M., Marien C. S., Kurzweil F., Van Kranendonk M. J., Smithies R. H., Maier W. D. and Garbe-Schönberg D. (in review) Convective isolation of Hadean mantle reservoirs through Archean time. *PNAS*

Van Kranendonk M. J. (2010) Two types of Archean continental crust: Plume and plate tectonics on early earth. *Am. J. Sci.* **310**, 1187–1209.

Van Kranendonk M. J., Collins W. J., Hickman A. and Pawley M. J. (2004) Critical tests of vertical vs. horizontal tectonic models for the Archaean East Pilbara Granite-Greenstone Terrane, Pilbara Craton, Western Australia. *Precambrian Res.* **131**, 173–211.

Van Kranendonk M. J., Hickman A. H., Smithes R. H. and Nelson D. R. (2002) Geology and tectonic evolution of the Archean North Pilbara Terrain, Pilbara Craton, Western Australia. *Econ. Geol.* **97**, 695–732.

Van Kranendonk M. J., Hugh Smithies R., Hickman A. H. and Champion D. C. (2007) Review: Secular tectonic evolution of Archean continental crust: interplay between horizontal and vertical processes in the formation of the Pilbara Craton, Australia. *Terra Nov.* **19**, 1–38.

Van Kranendonk M. J., Hugh Smithies R., Hickman A. H., Wingate M. T. D. D. and Bodorkos S. (2010) Evidence for Mesoarchean (~3.2 Ga) rifting of the Pilbara Craton: The missing link in an early Precambrian Wilson cycle. *Precambrian Res.* **177**, 145–161.

Van Kranendonk M. J., Smithies R. H., Griffin W. L., Huston D. L., Hickman A. H., Champion D. C., Anhaeusser C. R. and Pirajno F. (2015) Making it thick: a volcanic plateau origin of Palaeoarchean continental lithosphere of the Pilbara and Kaapvaal cratons. *Geol. Soc. London, Spec. Publ.* **389**, 83–111.

Vervoort J. D. and Blichert-Toft J. (1999) Evolution of the depleted mantle: Hf isotope evidence from juvenile rocks through time. *Geochim. Cosmochim. Acta* **63**, 533–556.

Vervoort J. D., Patchett P. J., Albarède F., Blichert-Toft J., Rudnick R. and Downes H. (2000) Hf-Nd isotopic evolution of the lower crust. *Earth Planet. Sci. Lett.* **181**, 115–129.

Wiemer D., Schrank C. E., Murphy D. T., Wenham L. and Allen C. M. (2018) Earth's oldest stable crust in the Pilbara Craton formed by cyclic gravitational overturns. *Nat. Geosci.* **11**, 357–361.

Willbold M. (2007) Determination of Ce isotopes by TIMS and MC-ICPMS and initiation of a new, homogeneous Ce isotopic reference material. *J. Anal. At. Spectrom.* **22**, 1364–1372.

Willig M. and Stracke A. (2019) Earth's chondritic light rare earth element composition: Evidence from the Ce–Nd isotope systematics of chondrites and oceanic basalts. *Earth Planet. Sci. Lett.* **509**, 55–65. Available at: https://doi.org/10.1016/j.epsl.2018.12.004.

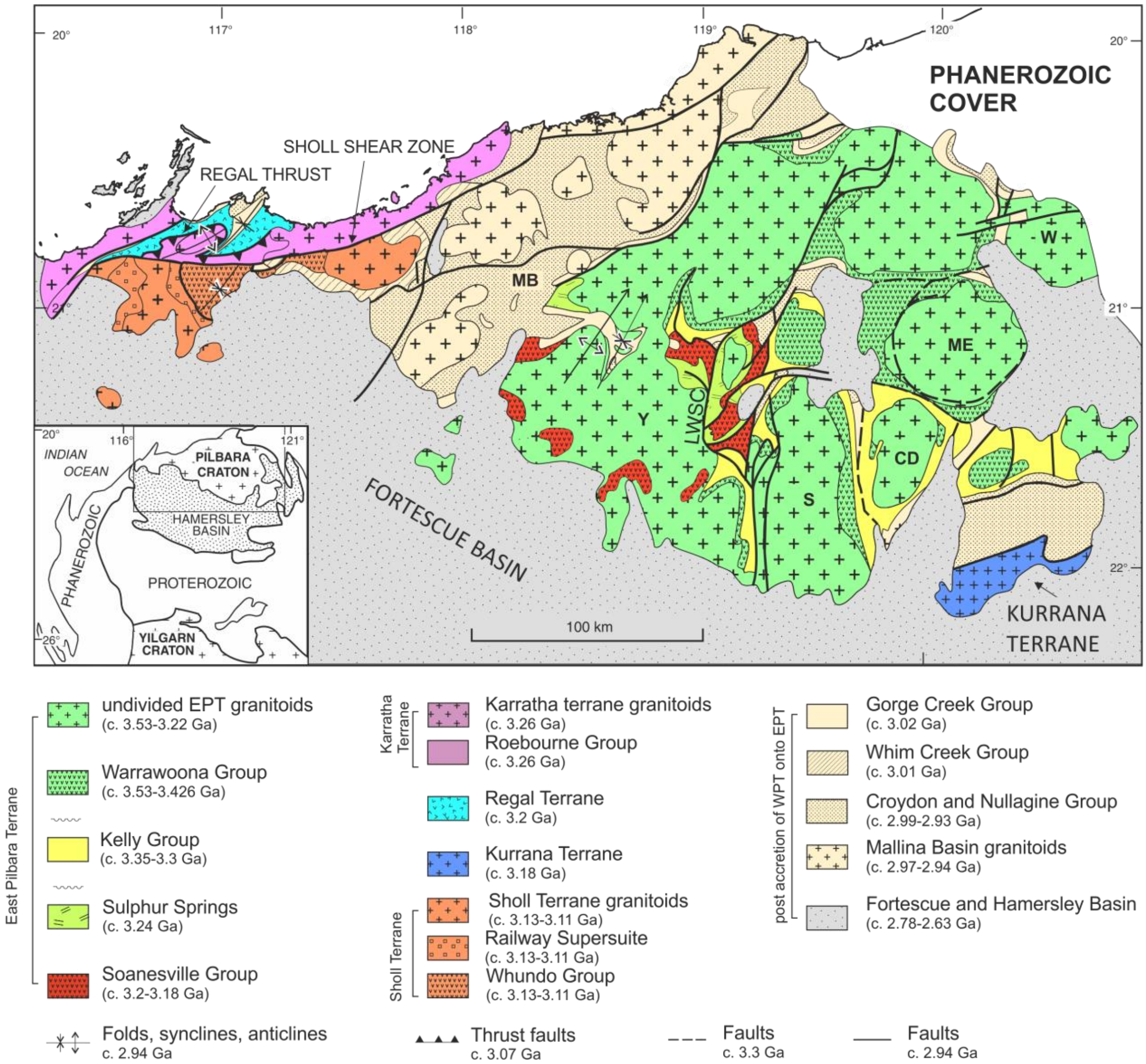

Fig. 1: Simplified geological map of the northern Pilbara Craton, showing greenstones and granitoids of the East Pilbara Terrane, Kurrana Terrane, Karratha Terrane, Regal Terrane, Sholl Terrane and the late volcano-sedimentary Mallina Basin and De Grey Supergroup (MB=Mallina Basin; MCB=Mosquito Creek basin) and Fortescue Basin. Abbreviations for different granitoids that were sampled in this study: CD=Corunna Downs; ME=Mount Edgar; S=Shaw; W=Warrawagine; Y=Yule. Modified after Van Kranendonk et al., (2007a), (2010).

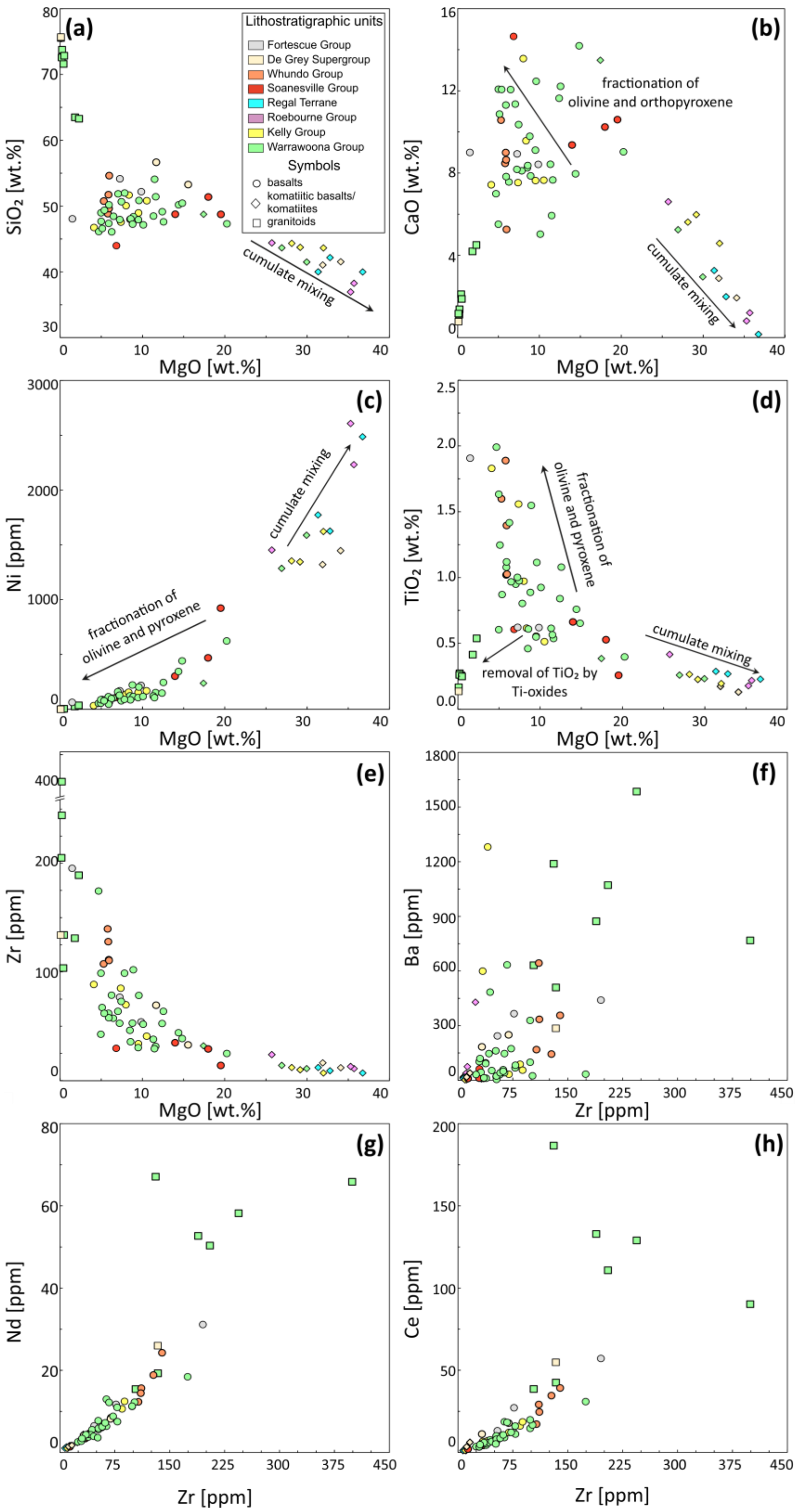

Fig. 2: Co-variation diagrams for selected major and trace elements in mafic-ultramafic to felsic Pilbara Craton samples a) - e) Selected major and trace elements plotted against MgO demonstrate the preservation of pristine igneous fractionation trends. f) Barium vs. Zr plot illustrating post-magmatic disturbances of large ion lithophile elements. g) and h) show preserved igneous trends for Ce, Nd and Hf (not shown) with Zr, implying that the elements relevant for radiogenic isotope measurements have preserved their pristine igneous composition. Shown symbols also include data from Maier et al., (2009) and Tusch et al., (2020) for samples that were also analyzed in this study.

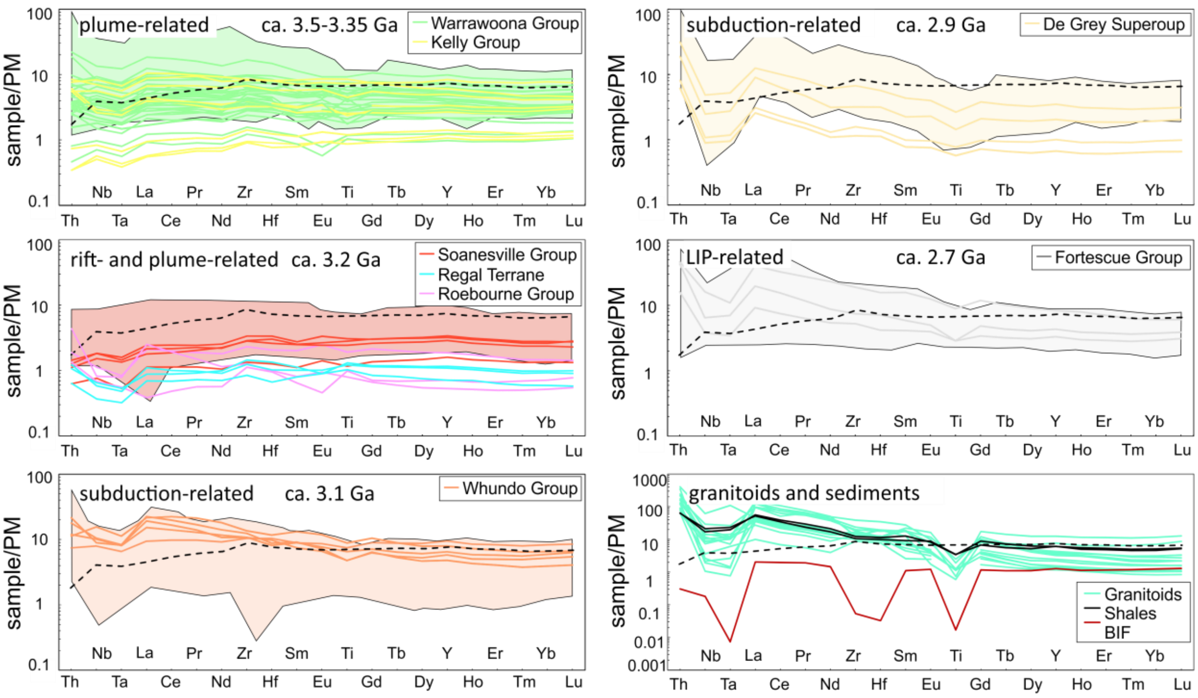

Fig. 3: Primitive mantle (PM) normalized incompatible trace element patterns for selected stratigraphic units, rock types, and geological settings. Additional data from Tusch et al., (2020) for samples that were also analyzed in this study. Colored fields represent compiled literature data. Detailed references for mantle reservoirs shown here are given in supplementary file S0.

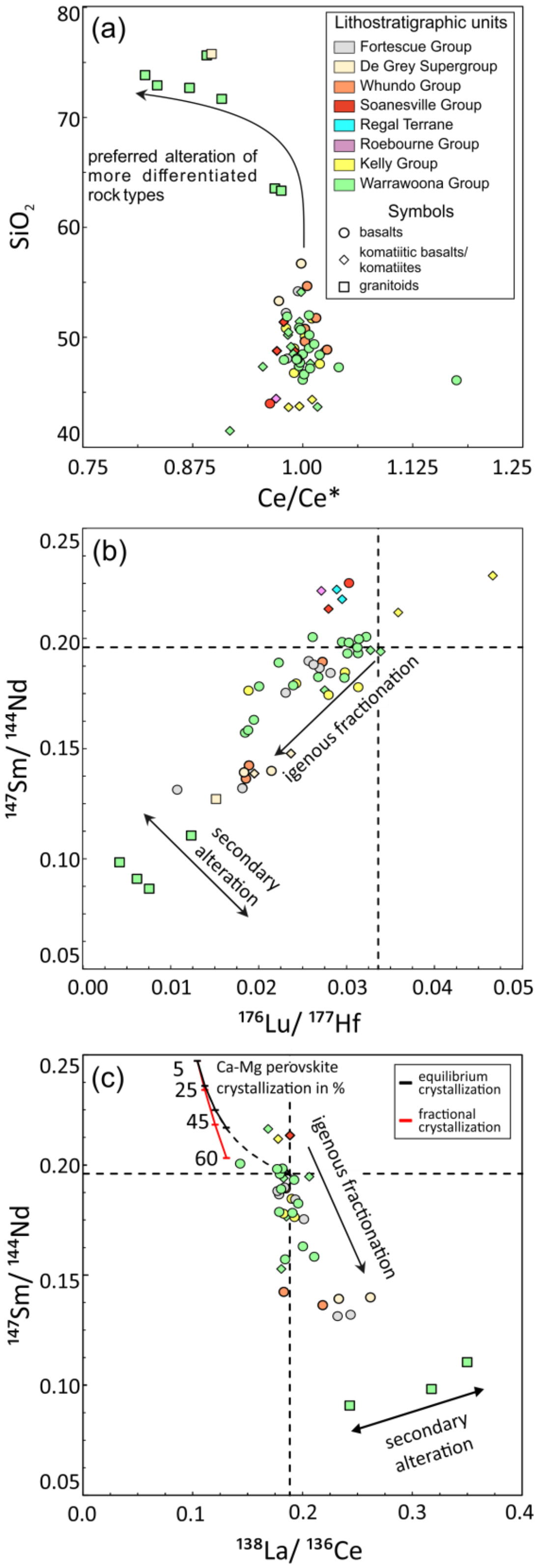

Fig. 4: Plots illustrating alteration features in Pilbara rocks. a) Ce/Ce* anomalies increase with increasing SiO_2. b) and c) co-variations of parent/daughter ratios of relevant radiogenic isotope systems indicate, that the majority of samples have preserved their pristine magmatic geochemistry. Additional data from Tusch et al., (2020) for samples that were also analyzed in this study.

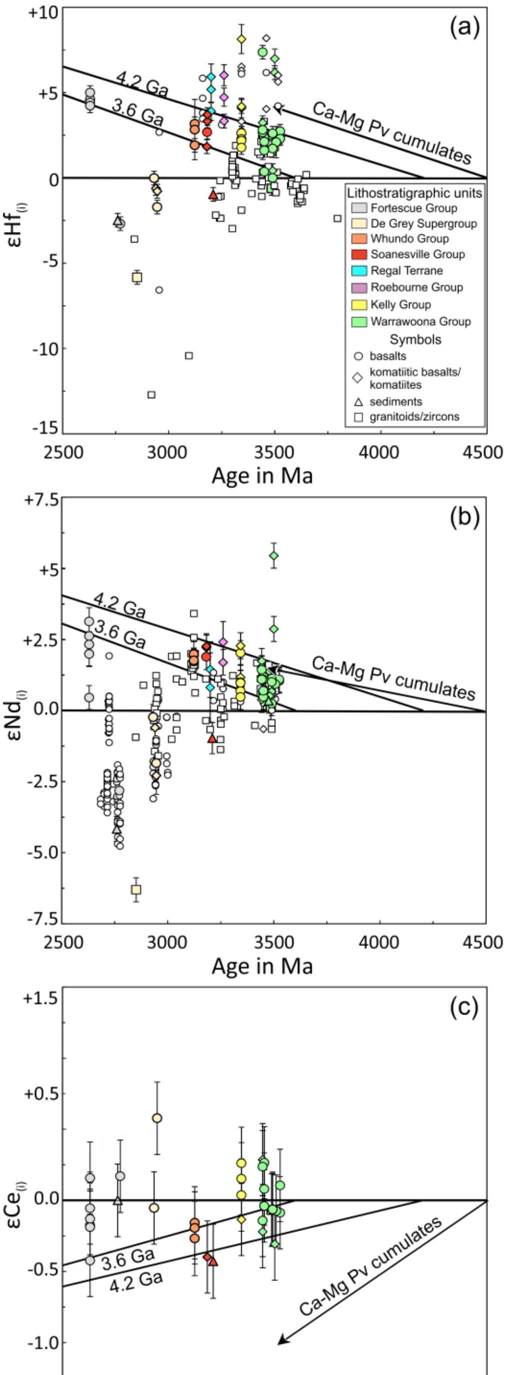

Fig. 5: Evolution of radiogenic isotope compositions in Pilbara rocks through geologic time. Panels illustrate a) initial Hf, b) initial Nd, and c) initial Ce isotope compositions. For Hf and Nd isotope compositions, our samples show a constant increase between ca. 3.59-3.18 Ga for most samples with the marked exception of the majority of 3.34 Ga Kelly Group samples. After 3.12 Ga, the Pilbara Craton develops towards more radiogenic Ce and less radiogenic Nd and Hf isotope compositions, reflecting a subduction-like setting and/or crustal contamination of older felsic crust. Additional literature data from the Pilbara Craton are shown here with smaller symbol sizes and without colors. Detailed references for literature data shown here are given in supplementary file S0. Errors are only shown for samples of this study and include the propagated errors of the external reproducibility on isotope composition measurements, measured parent/daughter ratios and the errors of the crystallization age of each specific formation. If the individually measured 2 S.E. was larger than the external reproducibility, we chose this error for the error propagation.

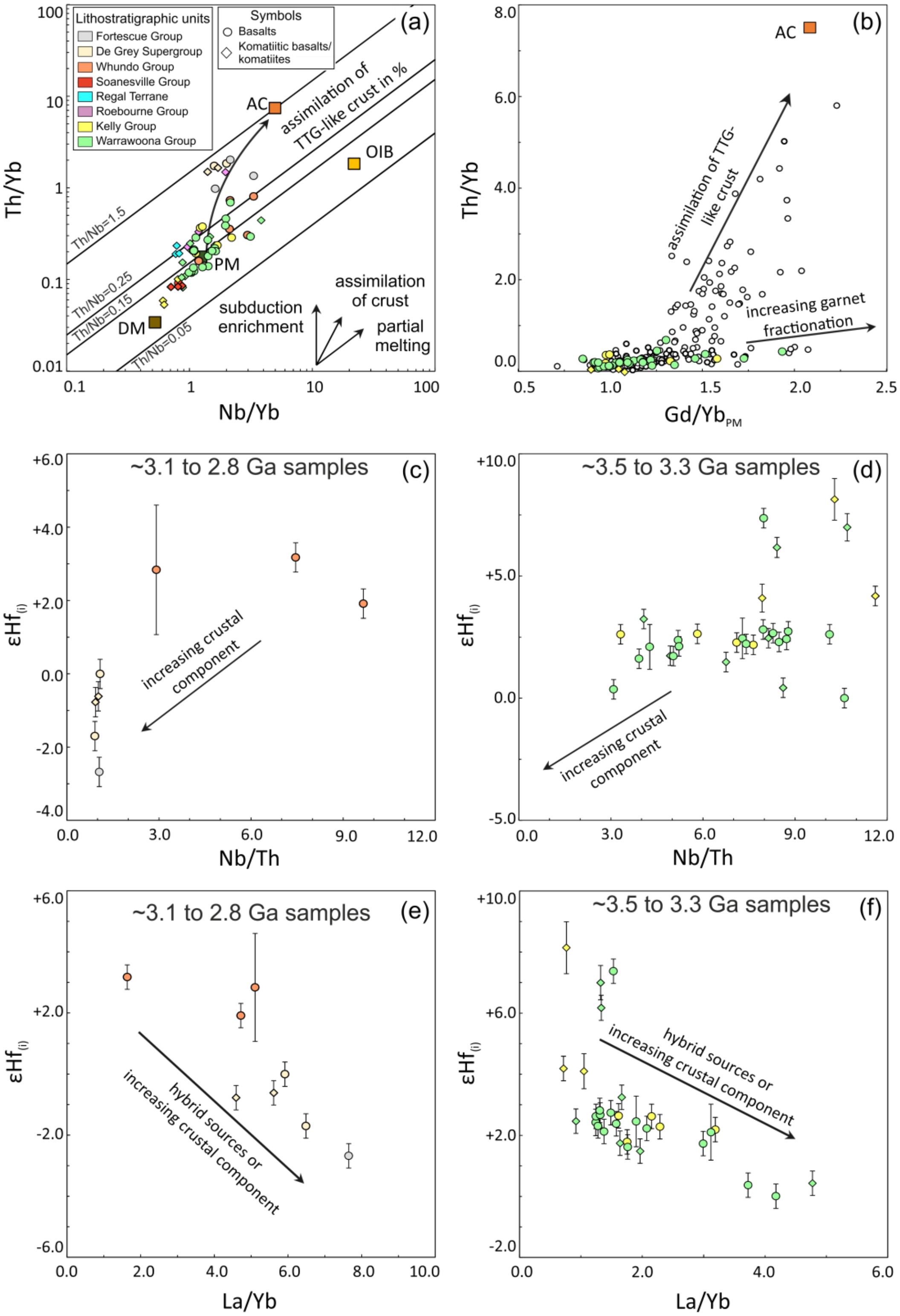

Fig. 6: Isotope and trace element variations illustrating effects of crustal contamination for selected suites. a) All ≤2.9 Ga samples b) but only some Paleoarchean samples have inherited an enriched component with high Th/Yb. c) and d) Hybrid mantle sources are likely responsible for decreased $\varepsilon Hf_{(i)}$ values of some EPT samples and not continental crust, as no co-variations between $\varepsilon Hf_{(i)}$ or $\varepsilon Nd_{(i)}$ with Nb/Th are observed, e) and f) but with La/Yb. Co-variations of $\varepsilon Hf_{(i)}$ with La/Yb and Th/Nb in younger successions, however, indicate mixing with crustal components rather than hybrid mantle sources. Additional literature data are taken from Tusch et al., (2020) for samples of this study. Additional literature data from the Pilbara Craton are shown here with smaller symbol sizes and without colors. Detailed references for literature data and various mantle reservoirs shown here (DM=depleted mantle, PM=primitive mantle, OIB=ocean island basalt, AC=Archean TTG-like crust), are given in supplementary file S0. Error estimates are the same as in Figure 5.

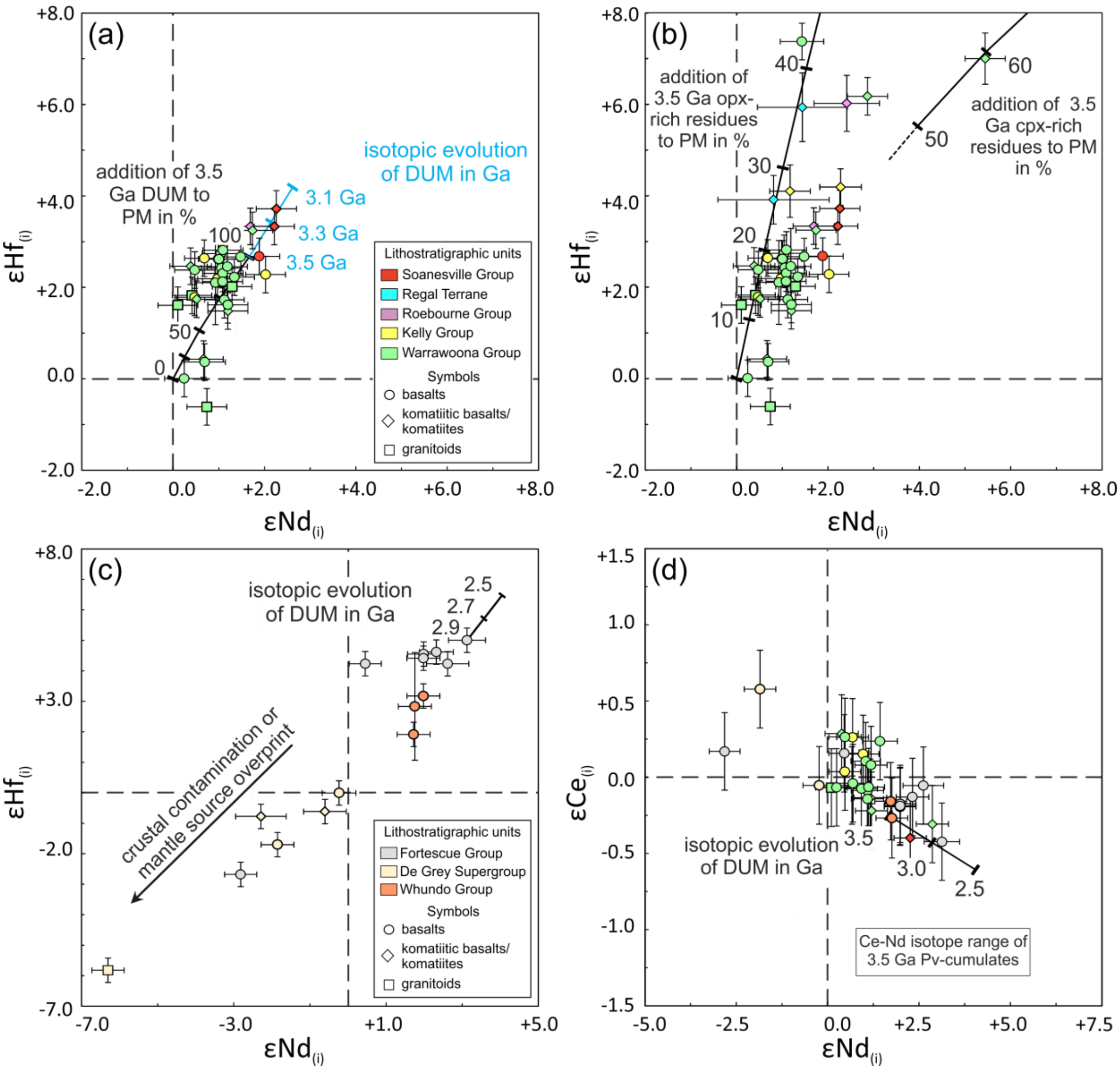

Fig. 7: Co-variation diagrams between initial Ce, Nd and Hf isotope compositions. a) $\varepsilon Hf_{(i)}$ vs. $\varepsilon Nd_{(i)}$ for 3.53-3.12 Ga samples show an increase of initial $\varepsilon Hf_{(i)}$ and $\varepsilon Nd_{(i)}$ values for most mafic samples with time that is best explained by an evolving depleted upper mantle (DUM) component. b) Some samples, in particular komatiites, are decoupled in their $\varepsilon Hf_{(i)}$ and $\varepsilon Nd_{(i)}$ composition, which is best explained by mixing of primitive mantle with older (~4.2 Ga) residual mantle domains showing decoupled Hf-Nd isotope compositions due to residual garnet. c) Refertilization of the mantle source or crustal contamination can explain the decreased $\varepsilon Hf_{(i)}$ vs. $\varepsilon Nd_{(i)}$ values found in some 2.94-2.63 Ga samples. d) Values of $\varepsilon Ce_{(i)}$ vs $\varepsilon Nd_{(i)}$ of unaltered samples show a coherent evolution compared to the $\varepsilon Hf_{(i)}$ and $\varepsilon Nd_{(i)}$ trend. Importantly, the Hf-Nd-Ce arrays defined by the Pilbara samples all overlap the chondritic value, with an Hf-Nd array for coupled samples of $\varepsilon Hf_{(i)}$= 1.2 (±0.2) × $\varepsilon Nd_{(i)}$ + 0.53 (±0.6) that is indistinguishable from the modern day Hf-Nd mantle array. The Ce-Nd array is defined by: $\varepsilon Ce_{(i)}$ =-0.14 (±0.07) × $\varepsilon Nd_{(i)}$ -0.08 (±0.3) and also overlaps with the present day Ce-Nd array (Israel et al., 2019). Error estimates are the same as in Figure 5.

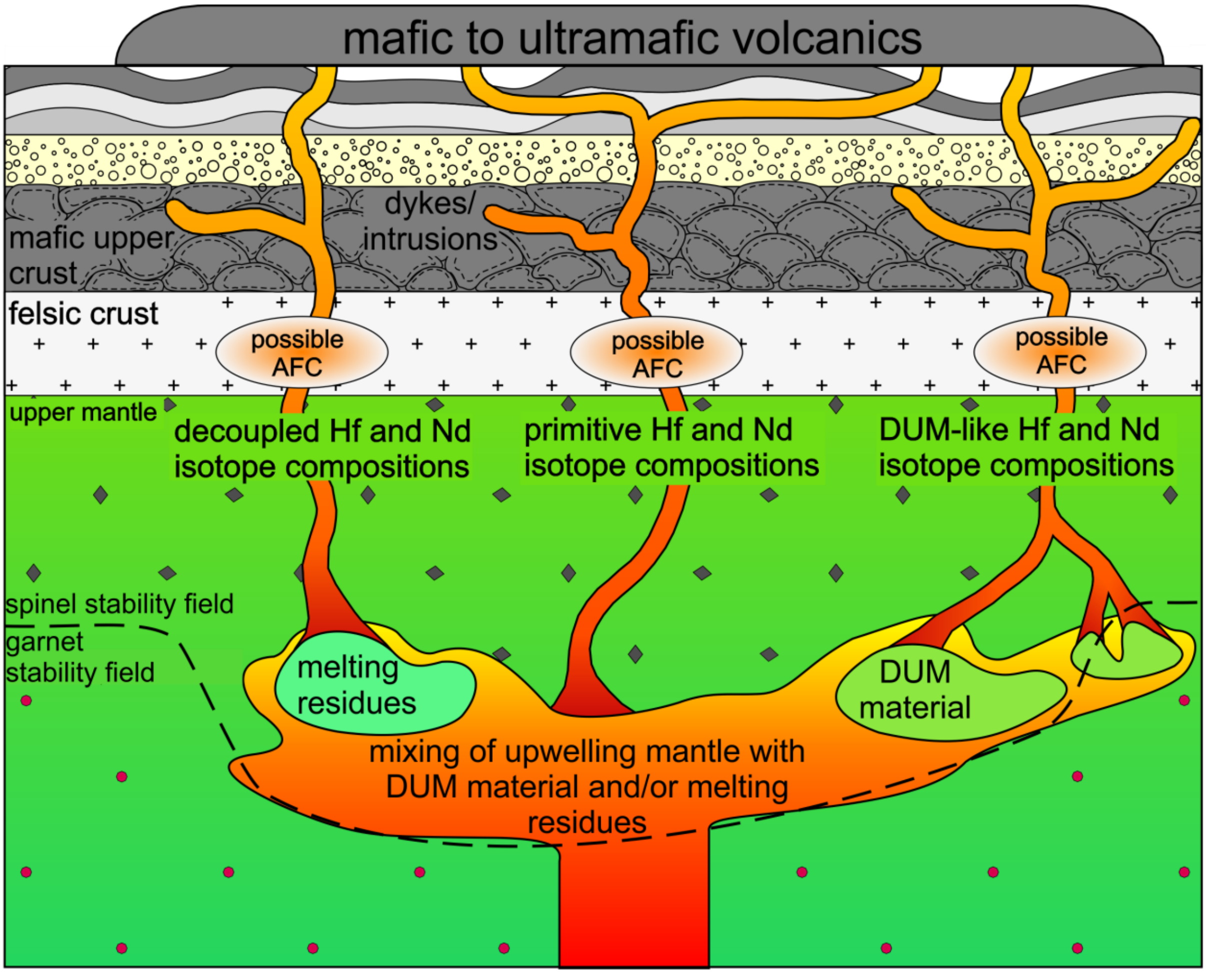

Fig 8: Sketch illustrating our proposed geodynamic model for the early evolution of the Pilbara craton as preserved in the EPT. Between ca. 3.5 to 3.3 Ga, near-primitive upwelling mantle mixes with ca. 4.2 Ga old depleted upper mantle (DUM) material and in some cases with residual mantle domains depleted in the garnet stability field. With such hybrid mantle sources (near primitive and garnet-bearing residual mantle domains), the pooled melts may have decoupled Hf-Nd isotope compositions. In contrast, mixing of near-primitive and DUM material (which is most frequent) generates melts that are not decoupled in their Hf and Nd isotope composition and lie in $\varepsilon Hf_{(i)}$ vs. $\varepsilon Nd_{(i)}$ space somewhere between primitive mantle and DUM recalculated to the time of eruption. Furthermore, the eruption of near-primitive mantle melts that have not mixed with residual domains or DUM material also occurred, although this compositional type must have been rare as only few samples are characterized by near-chondritic Hf and Nd isotope compositions.